Nondestructive Characterization of Graphene Defects

*Thuc Hue Ly, Dinh Loc Duong, Quang Huy Ta, Fei Yao, Quoc An Vu, Hye Yun Jeong, Sang Hoon Chae, and Young Hee Lee**

An effective method is reported for oxidizing graphene/copper film in which air oxidation of the underlying copper film occurs through the grain boundary lines of graphene without oxidizing graphene. This oxidation is realized by partially immersing the graphene/copper film in sodium chloride solution. Electrons generated during etching of the graphene/copper film in electrolyte diffuse into the film in contact with air, which eventually enhances air oxidation of copper through the graphene layer. While the graphene layer acts as a protective layer against oxidation of the copper film, oxidation of the underlying Cu film near graphene grain boundary lines is observed by optical microscopy. This observation could be attributed to the selective diffusion of oxygen radicals through isolated defects and graphene grain boundaries. The process involves no appreciable oxidation of the graphene layer including the graphene grain boundary, as confirmed by use of detailed Raman and X-ray photoelectron spectroscopy.

1. Introduction

Large-area graphene prepared on substrates such as Ni and Cu by chemical vapor deposition (CVD) has attracted considerable attention from basic science and industry.[1–3] Unlike highly oriented pyrolytic graphite (HOPG), CVD-grown graphene is highly defective with multigrains of different orientations.[4,5] CVD-grown monolayer graphene transferred onto a metal surface acts as a protective layer against oxidation of the metal in air.[6–8] Corrosion of metals in electrolyte is prevented by overlapping them with several monolayers of graphene, although Li ion diffusion perpendicular to the graphene plane occurs through defects that are formed on CVD-grown graphene layers.[9] It has been demonstrated that the sheet resistance of CVD-grown graphene is inversely proportional to the diameter of the graphene grain size.[10] Control of point defects, domain orientation, and grain boundaries are key factors in determining the electronic properties of graphene and optimizing the related device performance.

Another complication arises from observing such defects. Scanning tunneling microscopy (STM) can provide information of point defects on an atomic scale.[11,12] Transmission electron microscopy (TEM) combined with electron diffraction can be used to identify the location of the graphene grain boundary (GGB) on an atomic scale and the formation of various crystal orientation patterns of graphene domains.[13–17] Nevertheless, the extension of this information to macroscopic device performance has been limited. Recently, observation of GGB lines was realized by simple optical microscopy.[10] Although this method was capable of providing sheet resistance by measuring graphene domain sizes through oxidation of the graphene/Cu layer, oxidation of the top graphene layer inevitably occurred, which is a drawback for nondestructive in situ monitoring of graphene quality.[10]

The primary purpose of this work is to find a nondestructive method to observe the grain boundary of graphene that does not induce oxidation of the graphene layer. The nondestructive method of observing graphene grain boundary distribution in a macroscale presented here is very important in many aspects: i) Optical microscopes are easy to use and cheap so that every small lab can use them and in particular, this approach should be useful in industry as an easy test on the production line, ii) nondestructive observation is necessary since the grain boundary information can be correlated to macroscopic sheet resistance and also some other spectroscopic results such as Raman, absorption, transient absorption spectroscopies simultaneously, i.e., position-correlated spectroscopic results can be obtained to avoid misinterpretation of the data. If the graphene is damaged during oxidation, such additional investigation will not be possible. Our strategy is to enhance oxidation exclusively underneath the Cu film through the GGB by electron injection in air supplied from the etching process through immersion of half of the graphene/Cu film in NaCl solution. The immersed graphene/Cu film in NaCl solution generates electrons by corrosion of the Cu film. The generated electrons diffuse to the upper portion of the graphene/Cu film which enhances air oxidation of Cu film through GGBs under ambient moisture conditions. The underlying Cu film near the GGB lines in air is oxidized by a selective diffusion of oxygen radicals through GGBs and broadened to be observable by optical microscopy

T. H. Ly, Dr. D. L. Duong, Q. H. Ta, F. Yao, Q. A. Vu, H. Y. Jeong, S. H. Chae, Prof. Y. H. Lee
Center for Integrated Nanostructure Physics
Institute for Basic Science
Department of Energy Science, BK21 Physics Division
and Center for Nanotubes
and Nanostructured Composites
Sungkyunkwan University (SKKU)
Suwon 440-746, S. Korea
E-mail: leeyoung@skku.edu

DOI: 10.1002/adfm.201300493

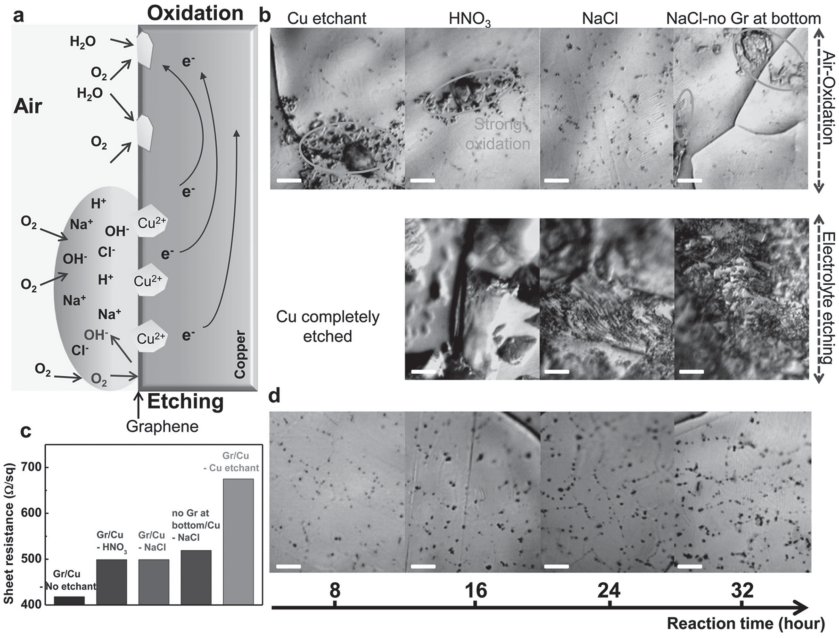

Figure 1. a) Schematic diagram for enhanced oxidation of copper in air through the GGB near the air/electrolyte interface. b) Optical microscopy images of graphene/Cu film with various solutions of Cu etchant (10%), HNO_3 (7%), NaCl (3%), and NaCl (3%) without graphene in the solution. The top and bottom panels are images from the centers of the air-oxidized and etchant-immersed regions. Air humidity was 43%. c) Sheet resistances of the treated graphene in various solutions for 24 h after transfer to a SiO_2 substrate. d) Reaction time dependence of images in NaCl solution. Scale bar represents 4 μm.

but no appreciable oxidation of graphene occurrs during this process, unlike the previously reported UV oxidation process.[10] This result is confirmed by using confocal Raman mapping and XPS analysis. Slow oxidation is a key factor for nondestructive observation of the GGB.

2. Results and Discussion

Figure 1a shows a schematic of the enhanced oxidation of graphene/Cu film in air assisted by electrons generated from etching of the lower portion of the graphene/Cu film. Four edges of graphene on Cu film were sealed with a Scotch tape and the bottom Cu surface was fully covered with polyethylene terephthalate (PET)/parafilm to avoid direct contact of the Cu film with the electrolyte (see Figure S1 in the Supporting Information). Half the sample was then immersed vertically into NaCl solution so that only the central portion of the graphene surface was exposed to electrolyte, while the parafilm-covered Cu film was fully protected from unnecessary chemical reaction. The submerged portion in electrolyte was 2 mm with an upper portion in air of greater than 10 mm. On the immersed portion of the graphene/Cu, copper was slowly corroded through a pitting process[18–20] that released copper ions and electrons. The enhanced oxidation of Cu film in air included two steps: pit corrosion[19] of the immersed graphene Cu film involving Cu wet etching and enhanced moisture-assisted oxidation in air of the upper portion of the film by diffused electrons from wet oxidation. The mechanism of pit growth includes anodic reactions inside the pit: $Cu \rightarrow Cu^{2+} + 2e^-$. Generated electrons diffuse to the upper portion of the film, as shown in Figure 1a. Oxidation in the upper portion continues by absorption of moisture and oxygen from air via the well-known air oxidation reaction: $½O_2 + H_2O + 2e^- \rightarrow 2OH^-$, which eventually forms copper hydroxide. The region of oxidized Cu film below the defective GGB expanded to several hundred nanometers, allowing observation of GGBs by optical microscopy. The CVD-grown monolayer graphene on the Cu surface acts as a protective layer against metal oxidation both in air and electrolyte.

To understand the roles of graphene and electrolyte in the Cu oxidation process, several electrolytes were examined with/without the presence of graphene. In this study, the CVD-grown graphene on copper foil was used directly without transfer. In the case of Cu etchant ($FeCl_3$ solution), the Cu film immersed in electrolyte was completely etched away even though the sample was completely sealed and protected by a graphene layer. Even the upper portion of the film in air was strongly etched, as evidenced in the severely etched region from the optical image in the upper panel of Figure 1b. Similar behavior was observed for HNO_3 solution, although in this case, the immersed portion of the Cu film was etched but intact. On the other hand, with NaCl solution, no severe Cu oxidation was observed in the upper portion of the film, but the immersed portion of the Cu film was still severely etched. The use of a high concentration of NaCl solution up to 35% did not cause severe Cu etching in the upper part of the film, which clearly differs from the results with HNO_3 solution (7%). To determine the effect of the presence of graphene in electrolyte solution, graphene was removed from the bottom portion of the film, which was placed in 3% NaCl solution. This action led to severe etching not only in the bottom portion of Cu film but also in the upper portion of the Cu film; this result is similar to the strong etching conditions of Cu etchant and HNO_3 solution. This result again indicates that graphene plays the role of a protecting layer in the electrochemical reaction, in agreement with previous observations.[8] Thus, single-layer graphene slows down electrochemical reactions in solution and reduces electron spillover to the upper portion of the film, although reactions still occur through point defects, (and/or) small voids, and GGBs. The slow reaction of Cu etching in the presence of a graphene overlayer, which is a key factor in minimizing severe damage on the upper portion of the graphene/Cu film, limits electron spillover and therefore controls the etching dynamics of the upper portion of the graphene/Cu film. Thus the presence of a graphene overlayer allows selective etching of the underlying Cu film through defective sites in the graphene.

The sheet resistance of the air-oxidized portion of graphene, measured after transfer onto a SiO_2 substrate, showed strong correlation with the dipping solutions. For instance, Cu etchant,

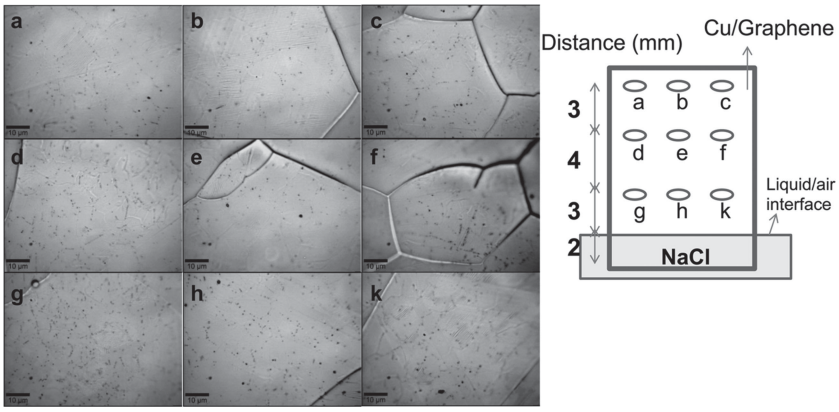

Figure 2. Positional dependence of the etching pattern of graphene/Cu film in air with a humidity of 43%. The bottom portion of the sample was immersed in 35% NaCl solution for 8 h. The corresponding positions were indicated in the right side. The etching behavior as a function of distance from liquid/air interface was nearly independent of the position from the interface.

which was the strongest etchant among the solutions used, gave the highest sheet resistance of 675 ohm sq^{-1}, which indicates strong oxidation of the graphene layer during the reaction, presumably causing graphene damage. The sheet resistance of graphene treated in HNO_3 solution was 499 ± 10 ohm sq^{-1}, similar to that of the graphene in NaCl but significantly larger than the 418 ± 5 ohm sq^{-1} value of pristine sample. These two solutions are rather mild etchants compared to Cu, from the view point of sheet resistance of graphene, although severe etching was also observed in HNO_3 solution. To see the effect of the graphene overlayer, the graphene layer in the bottom solution was removed by means of mechanical polishing with sand paper. The sheet resistance in this case increased to 519 ± 10 ohm sq^{-1}, which is larger than the 499 ohm sq^{-1} value of the sample before polishing. This result implies that graphene plays a protective layer against etching of copper film in electrolyte, in good agreement with a previous report.[4] Independent of the etchant used, the bottom graphene/Cu in electrolyte was severely damaged as shown in the bottom panels of Figure 1b. Four facts are noted: i) Except for the Cu etchant, the sheet resistance after solution treatment is not significantly altered, ii) 3% NaCl solution provides mild conditions to partially oxidize the air-exposed graphene/Cu film and eventually generate patterns in the GGBs, iii) the presence of a protective graphene layer particularly for the immersed film portion is critical to controlling electron spillover and therefore reaction dynamics, and iv) graphene is partially oxidized in NaCl and oxidation conditions need to be optimized to minimize the damage on graphene.

Our next step was to use mild NaCl solution to enhance the selective oxidation of the underlying Cu film through GGBs without promoting oxidation of graphene. The selective oxidation of Cu foil through the GGB was dependent on the oxidation concentration through changes in reaction time (Figure 1d), NaCl concentration (Supporting Information Figure S2), and environmental humidity (Supporting Information Figure S3). Black spots on the air oxidation region with 43% humidity began to appear after 8 h of dipping the graphene/Cu film in 35.8% NaCl solution. As the reaction time was increased to 24 h, the GGB lines were clearly visible. A longer reaction time of 32 h showed no further enhancement of the observed GGB pattern. **Figure 2** shows the etching behavior as a function of distance from liquid/air interface. No significant difference in the etching behavior was observed independent of the distance from the liquid/air interface, which is ascribed to the high conductivity of Cu film. Hence, as optimized conditions to observe the GGBs we chose a 24 h reaction time with a humidity of 62%.

GGBs are not visible with optical microscopy regardless of the substrate because of the nanoscale width of the boundaries,[4–6] although traces of the Cu grain boundaries on graphene are clearly observable because of their wide boundary width. **Figure 3**a shows an optical image of the upper portion of the oxidized graphene/Cu with 3% NaCl solution after 24 h in 62% air humidity. GGB lines are well visualized with clear thick Cu grain boundary lines in the left corner. The magnified region also clearly shows radial patterns centered at the nucleation seed (black spot), which explains the existence of several domains with different crystal orientations within the grain, in agreement with previous reports.[10,13] This nucleation seed could be formed with isolated point defects or small-sized voids depending on

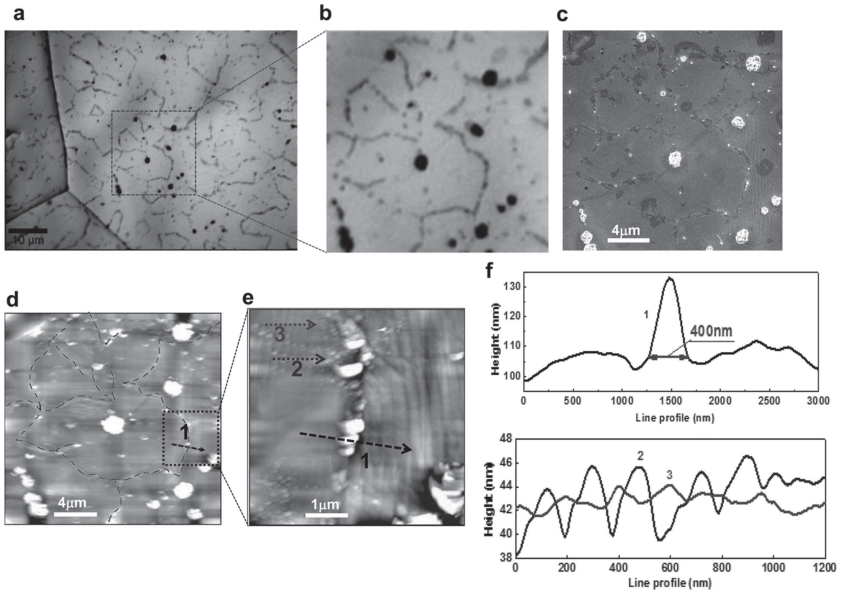

Figure 3. a,b) Optical images of oxidized graphene/Cu and the square magnified region. c) SEM image of the same magnified region as (b), d,e) AFM images of a region similar to (b) and the square magnified region, and f) height profile of lines 1, 2, and 3 shown in (e).

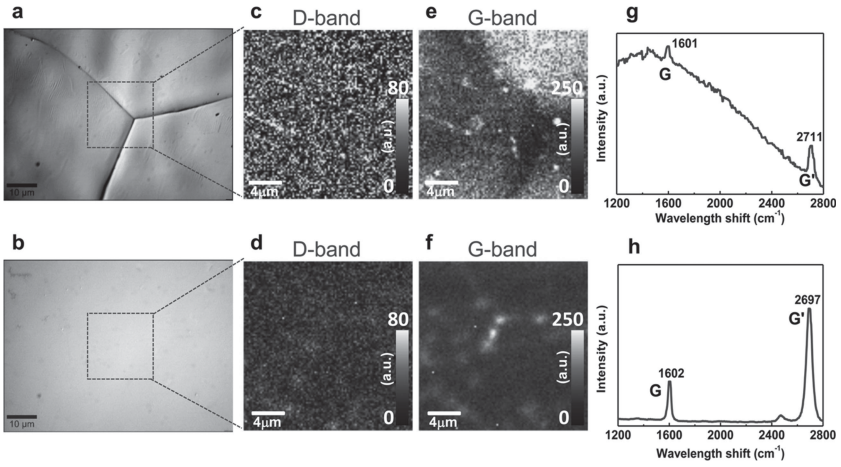

Figure 4. a, b) Optical images, c, d) D-band intensity mapping, e, f) G-band intensity mapping, and g,h) Raman spectra of pristine graphene on Cu film and on SiO_2/Si wafers, respectively.

the growth conditions. The formation of copper hydroxide (discussed later) near the GGB was also seen as dark lines in the field emission scanning electron microscopy (FESEM) image (Figure 3c and Supporting Information Figure S4). We emphasize here that our oxidation conditions were much milder than the previous UV oxidation,[10] but clear GGB patterns were still observed. Similar GGB patterns were also observed in atomic force microscopy (AFM) images in tapping mode (Figure 3d). The optical, SEM, and AFM images were perfectly matched. Figure 3f shows a height profile for several lines (Figure 3e): 1, across the GGB, 2, isolated point defects or small-size voids observed after oxidation, and 3, copper steps. The region of oxidized copper below GGBs expanded to approximately 400 nm in width, and therefore was observable with the optical microscope. We emphasize that the GGB could be composed of discrete small voids, as can be evidenced from AFM image (Figure 3f). Line profile 2 also revealed a repetition of peaks with a width of around 200 nm and a height of about 5 nm, visualized as a series of white spots, as shown in Figure 3e. This image certainly contrasted with the copper step lines 1–2 nm in height and 150–220 nm in separation distance, as shown in line profile 3. These dots were not visualized under optical microscope due to the limit of resolution. These dots are presumably point-defect related and will require further investigation.

We next investigated the oxidation of graphene that may occur during our process. Clear copper grain boundary lines are shown in the optical image of the pristine graphene/Cu sample, but no traces of grain boundary lines in graphene were visible (**Figure 4**a). The D-band and G-band Raman mappings showed no distinct traces of GGBs for either substrate (Figure 4c–4f). The CVD-grown graphene/Cu exhibited a large G′/G intensity ratio of 2.9 (Figure 4g) with strong background fluorescence from the copper substrate. After transfer onto a SiO_2/Si wafer, G-band and G′-band were clearly observed with a high aspect ratio of G′/G = 3, which is indicative of a high-quality graphene monolayer.[21–23] The G-band peak was slightly upshifted, whereas G'-band peak was downshifted compared with peaks from the graphene on copper film. Small bright spots are visible in Figure 4f, which could be ascribed to the multilayer portion formed at the nucleation seeds. Since no appreciable D-band intensity was developed near these bright spots, it is very unlikely that they are associated with edge functionalization of these islands.

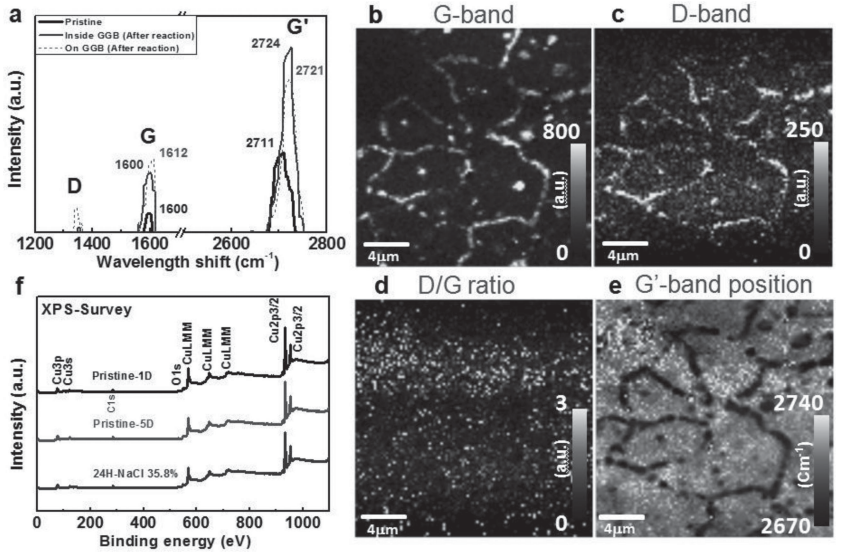

Figure 5. a) Raman spectra of oxidized graphene/Cu after subtraction of background fluorescence on different locations inside the GB and on the GB. Confocal Raman mapping of the same positions as Figure 2b for b) G-band intensity (1540–1640 cm^{-1}), c) D-band intensity (1300–1400 cm^{-1}), d) D/G intensity ratio, and e) G′-band position integrated over 2670–2740 cm^{-1}. f) XPS of pristine graphene/Cu (top), pristine sample exposed to ambient conditions for 5 days (middle), and a sample oxidized with 35.8% NaCl solution.

Raman spectra were obtained from two locations on the oxidized graphene/Cu, inside the grain and on the grain boundary (**Figure 5**a). In the case of the Raman spectrum from inside the grain, the small D-band was developed after oxidation but much smaller than that on the grain boundary. Furthermore, a G-band peak shift was not observed compared to the pristine sample and G/G' intensity ratio inside the grain was similar to that of pristine sample. These are in good contrast with previous work in which the D-band was developed and the G-band was upshifted inside the grain in the UV oxidation approach.[5] This difference again implies the nondestructive nature of our approach. On the other hand, in the case of the Raman spectrum taken on the grain boundary, relatively high D-band intensity was developed and more importantly G-band and G′-band peaks were upshifted due to oxidation, similar to in the UV oxidation approach.[5] The GGB line patterns were

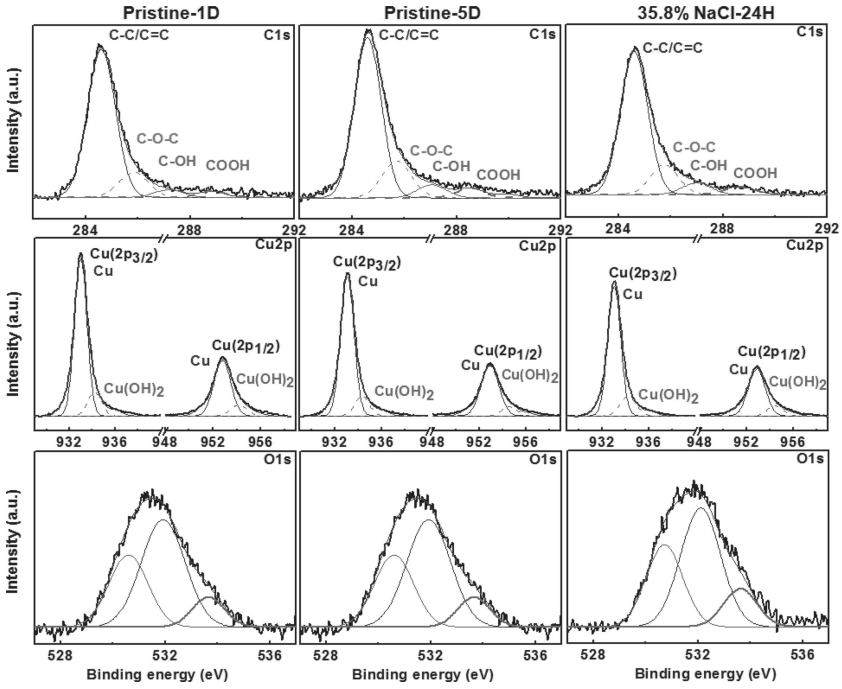

Figure 6. Distinction of the oxidation on graphene. XPS C1s (top), O1s (bottom), and Cu2p peaks (middle) of pristine graphene/Cu (Pristine-1D), a pristine sample exposed to ambient conditions for 5 days (Pristine-5D), and an oxidized sample from treatment with 35.8% NaCl solution for 24 h (35.8% NaCl-24H).

also confirmed using confocal Raman mapping of the G-band intensity, as seen in Figure 3b. Mapping of the D-band intensity and G′-band position also clearly demonstrated similar GG line patterns, as shown in Figure 5c,e. Interestingly, no distinct line pattern was observed in the D/G intensity ratio, but similar point defectlike dot patterns were observed both in the D/G ratio and G′-band position profile.

Oxidation was further confirmed by X-ray photoelectron spectroscopy (XPS) of three samples (Figure 5f): graphene oxidized for 1 day (Pristine-1D), 5 days (Pristine-5D) under our oxidation conditions, and oxidized with NaCl solution for 24 h in air with 35.8% humidity. It is important to note that in addition to oxidation of graphene by the formation of epoxide, hydroxy, and carboxy groups, the copper foil was also oxidized by forming exclusively $Cu(OH)_2$ and not CuO_x (**Figure 6**). The C1s peak exhibited long tails in the high energy side related to epoxide, carboxy, and hydroxy groups.[24] The $Cu2p_{1/2}$ and $Cu2p_{3/2}$ peaks for graphene/Cu before and after oxidation exhibited $Cu(OH)_2$ peaks at 955.1 and 934.8 eV, respectively.[8] Only the $Cu(OH)_2$ component appeared with the Cu2p peak.

Detailed data extracted from convolution of C1s, O1s, and Cu2p are summarized in **Table 1**, and the compositions of functional groups from C1s fitting are summarized in **Table 2**. The pristine sample with one-day exposure under ambient conditions had roughly 3.7% oxygen content due to probable adsorption of oxygen-related functional groups at defect sites. The oxygen content further increased to 5.1% after exposure for 5 days. It is notable that the current oxidation approach does not promote more severe oxidation than native oxidation after 5 days exposure under ambient conditions. A slight increase in oxidation was mainly due to oxidation of the copper substrate near the GGBs and not graphene oxidation, as was evident from the disappearance of the D-band profile after transfer of the graphene layer to a SiO_2 substrate (discussed later). A similar trend was observed in the C1s spectral analysis in Table 2. Hydroxy (C-OH), epoxy (C-O-C), and carboxy (COOH) groups from the current oxidation maintained similar or lower levels than those after 5 days of oxidation under ambient conditions, which again indicates that no further oxidation occurred with the current approach. Our results were also in strong contrast with a previous report that simple air oxidation under humid conditions initiated oxidation not only on the grain boundaries but also inside the graphene grain.[10]

To provide a proof of concept and demonstrate the power of our nondestructive approach, the graphene was transferred to SiO_2/Si wafers. Optical imaging and confocal Raman mapping were again used to confirm the GGBs (**Figure 7**). Cracks were not observed by optical microscope after transfer. Confocal Raman mapping of G-band and D-band intensity from graphene on SiO_2 substrate revealed patterns of white lines, which are distinct from the GGB patterns on Cu substrate observed in Figure 5. The origin of these bright lines is not clear at the moment and may be strain,[25] which is not observed using normal Raman signals but identified by near-field scanning optical micrsoscopy (NSOM)-Raman.[26] To confirm the quality of graphene, the sheet resistance of the optimized sample was measured to be 432 ± 5 ohm sq^{-1}; this value is similar to the 418 ± 5 ohm sq^{-1} value of the pristine graphene, to within statistical error. This result again indicates the nondestructive nature of our oxidation approach which clearly differs from the previous UV oxidation.[10]

3. Conclusions

In summary, we have studied a method for observing graphene grain boundaries by using optical microscopy, which does not damage the graphene layer. This technique was realized by enhancing oxidation of an underlying Cu film through the graphene grain boundaries in air by electron injection supplied by electrochemical reaction of the graphene/Cu film. The

Table 1. Detailed data extracted from deconvolution of C1s, O1s, and Cu2p peaks in XPS.

	Pristine-1D	Pristine-5D	Dip in 35.8% NaCl-24H
(C1s) C%	22.3	25.9	24.8
(O1s) O%	3.7	5.1	5.8
Cu%	74.0	69.0	69.4
O/(C+Cu)	0.04	0.05	0.06

Table 2. Composition of functional groups from C1s fitting.

	Pristine-1D	Pristine-5D	Dip in 35.8% NaCl-24H
C–C (sp^2)	79	71.4	73.9
C=OH	4	6.3	6.3
C–O=C	14	17.9	15.6
COOH	3	4.4	4.2
sp^3/sp^2	0.26	0.4	0.35

selective, slow oxidation in our method is a key factor for oxidizing the underlying Cu layer without promoting oxidation of the graphene. We further observed point defects inside the graphene grain with AFM. We expect that our approach could be exploited to observe point defects and grain boundaries, and furthermore, to control defect formation during growth.

4. Experimental Section

Sample Preparation: Enhanced air oxidation (EAOx) of graphene/copper at atmospheric pressure: Graphene on copper foil was prepared by atmospheric-pressure chemical vapor deposition (APCVD; see Supporting Information). The prepared graphene/Cu substrate was placed on PET/parafilm, and the four corners of the graphene/Cu film were fixed with Scotch tape. This sample was immersed perpendicularly into NaCl solution in a beaker as shown in the schematic of Supporting Information Figure S1. Special care was taken to avoid direct contact of the copper film with electrolyte. The NaCl solution in the beaker was sealed by parafilm to avoid unnecessary environmental effects on the oxidation of the portion of Cu film not in solution. The humidity level at atmospheric pressure was measured with a hydrothermometer (accuracy of ±5%).

Humid air undergoes the following reaction under EAOx with electrolyte reaction: $Cu \rightarrow Cu^{2+} + 2e^-$ and the generated electrons are transferred and further consumed by the air reaction: $½O_2 + H_2O + 2e^- \rightarrow 2OH^-$. The region of oxidized copper foil beneath the defective grain boundary of graphene expanded with the continuous supply of environment humidity through the grain boundary $½O_2 + H_2O + Cu^0 \rightarrow Cu(OH)_2$. Thus, generated OH^- group, in addition to O_2, can be the oxidizing agent.

Enhanced air oxidation of graphene/copper at controlled pressure in a closed quartz chamber: The sample was prepared as in Supporting Information Figure S1, and then the sealed beaker was placed in a quartz tube chamber. The chamber was connected to a water bubbler to introduce humidity into the chamber. The humidity level in the chamber was monitored using a hydrothermometer (accuracy of ±5%), and the chamber was continuously ventilated to maintain a constant pressure. After reaching the required humidity level, the water bubbler was disconnected from the chamber.

In our experiments, GGBs were not observed with humidity levels less than 30%, or with high humidity in the closed chamber (low O_2 concentration).

Optical Microscopy and Raman Spectroscopy: Optical microscopy (100× magnification, Olympus, Japan, numerical aperture = 0.9) was used to obtain images of the surface morphologies of graphene/Cu samples. 2D confocal Raman mapping (CRM 200, Witec, Germany) was also performed using a doubled Nd:YAG laser (532 nm) with 1 mW power to confirm optical imaging results. Scan images were obtained at 100 × 100 pixels with a grating of 600 g mm^{-1} to yield a spectral resolution of 5 cm^{-1}. The accumulation time for each spectrum was 0.3 s for image scanning and 30 s for a single spectrum. A sum filter was used to extract the D-band (1300–1400 cm^{-1}), G-band (1540–1640 cm^{-1}), and G'-band (2670–2740 cm^{-1}) distributions after copper background subtraction was performed.

Atomic Force Microscopy (AFM): AFM images were obtained using a SPA400 system (SEIKO, Japan) in tapping mode. A NSC14-type silicon tip (MikroMasch, Estonia) with an approximately 10-nm tip radius was used. In general, the force constant and resonant frequencies of the tips were approximately 5 N m^{-1} and 160 kHz, respectively.

Scanning Electron Microscopy (SEM) and Energy Dispersive Spectroscopy (EDS): Field-emission scanning electron microscopy (FESEM; JSM7000F, Jeol, Japan) was used to examine the surface morphology of samples at different accelerating voltages to obtain a high level of contrast at different magnifications. An X-Max Silicon Drift Detector in a FESEM-JSM7600F system was used for EDS mapping for 10 min. An accelerating voltage of 3 keV was used to obtain sufficiently pronounced signals while retaining sensitivity to the sample surface.

X-ray Photoelectron Spectroscopy (XPS): XPS was performed using an Al Kα X-ray source (XPS, ESCA2000, VG Microtech). C1s, Cu2p, O1s peak data were collected to analyze the extent of oxidation of the graphene and underlying Cu foil. X-ray photoelectron spectroscopy (QUANTUM 2000, Physical electronics, USA) was performed using focused monochromatic Al Kα radiation (1486.6 eV).

Sheet Resistance Measurements: Graphene was transferred onto a silicon wafer using a poly(methyl methacrylate) (PMMA)-supported layer as previously described.[5] Resistance was measured with a Keithley 2000 Multimeter using the four-point probe method.

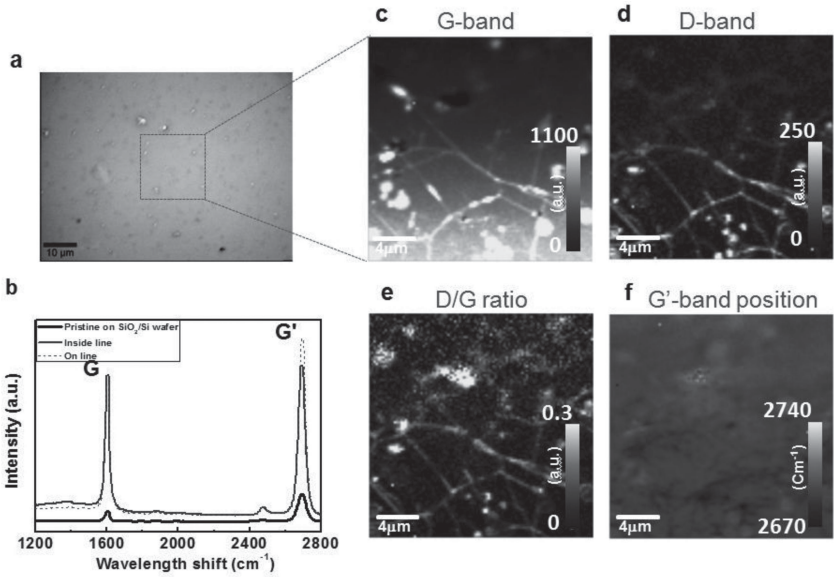

Figure 7. Confocal Raman mapping of oxidized graphene (Figure 2a) transferred onto a SiO_2/Si wafer. a,b) Optical images and Raman spectra of oxidized graphene after transfer to a SiO_2/Si wafer. c) G-band intensity mapping (1540–1640 cm^{-1}). d) D-band intensity mapping (1300–1400 cm^{-1}). e) D/G intensity ratio mapping. f) G'-band position mapping (2670–2740 cm^{-1}). No direct correlation of the white lines to the pattern of GGB lines observed from graphene on Cu was observed. The brighter lines in the intensity mapping profile may result from strain or wrinkles; they are not observed using normal Raman spectroscopy but identified by using NSOM-Raman.[26]

Electrochemical Measurements: Electrochemical measurements were performed with a three-electrode cell using a VMP3 instrument (BioLogic Science Instrument). A platinum wire was used as the counter electrode, Ag/AgCl was used as the reference electrode, and the sample of interest was used as the working electrode. The three electrodes were immersed in 3% NaCl electrolyte.

Supporting Information

Supporting Information is available from the Wiley Online Library or from the author.

Acknowledgements

This work was supported by the Research Center Program from IBS (Institute for Basic Science) in Korea, the Human Resources Development Program (No. 20124010203270) of the Korea Institute of Energy Technology Evaluation and Planning (KETEP) grant funded by the Korean Ministry of Knowledge Economy, and WCU Program through the National Research Foundation of Korea funded by the Ministry of Education, Science and Technology (R31-2008-10029).

Received: February 6, 2013
Revised: March 8, 2013
Published online: April 19, 2013

[1] S. J. Chae, F. Güneş, K. K. Kim, E. S. Kim, G. H. Han, S. M. Kim, H. J. Shin, S. M. Yoon, J. Y. Choi, M. H. Park, C. W. Yang, D. Pribat, Y. H. Lee, *Adv. Mater.* **2009**, *21*, 2328–2333.
[2] K. S. Kim, Y. Zhao, H. Jang, S. Y. Lee, J. M. Kim, K. S. Kim, J. H. Ahn, P. Kim, J. Y. Choi, B. H. Hong, *Nature* **2009**, *457*, 706–710.
[3] X. Li, W. Cai, J. An, S. Kim, J. Nah, D. Yang, R. Piner, A. Velamakanni, I. Jung, E. Tutuc, S. K. Banerjee, L. Colombo, R. S. Ruoff, *Science* **2009**, *324*, 1312–1314.
[4] P. T. Araujo, M. Terrones, M. S. Dresselhaus, *Mater. Today* **2012**, *15*, 98–109.
[5] G. H. Han, F. Güneş, J. J. Bae, E. S. Kim, S. J. Chae, H. J. Shin, J. Y. Choi, D. Pribat, Y. H. Lee, *Nano Lett.* **2011**, *11*, 4144–4148.
[6] D. Prasai, J. C. Tuberquia, R. R. Harl, G. K. Jennings, B. R. Rogers, K. I. Bolotin, *ACS Nano* **2012**, *6*, 1102–1108.
[7] R. K. Singh, P. C. Banerjee, D. E. Lobo, H. Gullapalli, M. Sumandasa, A. Kumar, L. Choudhary, R. Tkacz, P. M. Ajayan, M. Majumder, *Carbon* **2012**, *50*, 4040–4045.
[8] S. Chen, L. Brown, M. Levendorf, W. Cai, S. Y. Ju, J. Edgeworth, X. Li, C. W. Magnuson, A. Velamakanni, R. D. Piner, J. Kang, J. Park, R. S. Ruoff, *ACS Nano* **2011**, *5*, 1321–1327.
[9] F. Yao, F. Güneş, H. Q. Ta, S. M. Lee, S. J. Chae, K. Y. Sheem, C. S. Cojocaru, S. S. Xie, Y. H. Lee, *J. Am. Chem. Soc.* **2012**, *134*, 8646–8654.
[10] D. L. Duong, G. H. Han, S. M. Lee, F. Gunes, E. S. Kim, S. T. Kim, H. Kim, Q. H. Ta, K. P. So, S. J. Yoon, S. J. Chae, Y. W. Jo, M. H. Park, S. H. Chae, S. C. Lim, J. Y. Choi, Y. H. Lee, *Nature* **2012**, *490*, 235–239.
[11] J. Tian, H. Cao, W. Wu, Q. Yu, Y. P. Chen, *Nano Lett.* **2011**, *11*, 3663–3668.
[12] F. Banhart, J. Kotakoski, A. V. Krasheninnikov, *ACS Nano* **2011**, *5*, 26–41.
[13] P. Y. Huang, C. S. Ruiz-Vargas, A. M. van der Zande, W. S. Whitney, M. P. Levendorf, J. W. Kevek, S. Garg, J. S. Alden, C. J. Hustedt, Y. Zhu, J. Park, P. L. McEuen, D. A. Muller, *Nature* **2011**, *469*, 389–392.
[14] D. W. Kim, Y. H. Kim, H. S. Jeong, H. T. Jung, *Nat. Nanotechnol.* **2012**, *7*, 29–34.
[15] Q. Yu, L. A. Jauregui, W. Wu, R. Colby, J. Tian, Z. Su, H. Cao, Z. Liu, D. Pandey, D. Wei, T. F. Chung, P. Peng, N. P. Guisinger, E. A. Stach, J. Bao, S. S. Pei, Y. P. Chen, *Nat. Mater.* **2011**, *10*, 443–449.
[16] K. Kim, Z. Lee, W. Regan, C. Kisielowski, M. F. Crommie, A. Zettl, *ACS Nano* **2011**, *5*, 2142–2146.
[17] J. An, E. Voelkl, J. W. Suk, X. Li, C. W. Magnuson, L. Fu, P. Tiemeijer, M. Bischoff, B. Freitag, E. Popova, R. S. Ruoff, *ACS Nano* **2011**, *5*, 2433–2439.
[18] H. D. Yu, Z. Zhang, M. Y. Han, *Small* **2012**, *8*, 2621–2635.
[19] G. S. Frankel, *J. Electrochem. Soc.* **1998**, *145*, 2186–2198.
[20] H. P. Leckie, H. H. Uhlig, *J. Electrochem. Soc.* **1966**, *113*, 1262–1267.
[21] H. I. Rasool, E. B. Song, M. J. Allen, J. K. Wassei, R. B. Kaner, K. L. Wang, B. H. Weiller, J. K. Gimzewski, *Nano Lett.* **2011**, *11*, 251–256.
[22] C. Casiraghi, S. Pisana, K. S. Novoselov, A. K. Geim, A. C. Ferrari, *Appl. Phys. Lett.* **2007**, *91*, 233108.
[23] R. R. Nair, P. Blake, A. N. Grigorenko, K. S. Novoselov, T. J. Booth, T. Stauber, N. M. R. Peres, A. K. Geim, *Science* **2008**, *320*, 1308–1316.
[24] F. Güneş, G. H. Han, H. J. Shin, S. Y. Lee, M. Jin, D. L. Duong, S. J. Chae, E. S. Kim, F. Yao, A. Benayad, J. Y. Choi, Y. H. Lee, *NANO* **2011**, *06*, 409–418.
[25] R. He, L. Zhao, N. Petrone, K. S. Kim, M. Roth, J. Hone, P. Kim, A. Pasupathy, A. Pinczuk, *Nano Lett.* **2012**, *12*, 2408–2413.
[26] J. W. Suk, A. Kitt, C. W. Magnuson, Y. Hao, S. Ahmed, J. An, A. K. Swan, B. B. Goldberg, R. S. Ruoff, *ACS Nano* **2011**, *5*, 6916–6924.